



Binary and ternary adsorption equilibria for CO₂/CH₄/N₂ mixtures on Zeolite 13X beads from 273 to 333 K and pressures to 900 kPa

Ghazal Avijegon¹ · Gongkui Xiao¹ · Gang Li¹ · Eric F. May¹

Received: 30 December 2017 / Revised: 25 April 2018 / Accepted: 30 April 2018 / Published online: 9 May 2018
© Springer Science+Business Media, LLC, part of Springer Nature 2018

Abstract

Reliable adsorption equilibrium data and theoretical models for their accurate representation are crucial to the design of any adsorption based separation. The adsorption equilibria of carbon dioxide, methane and nitrogen are particularly important to the development of industrial pressure swing adsorption processes intended to separate CO₂ and N₂ from a variety of conventional as well as unconventional natural gas sources. The adsorption equilibrium capacities of gas mixtures needed for process design and simulation are often predicted from pure component adsorption data using various models including the ideal adsorbed solution theory (IAST). In this work, we present the adsorption equilibrium capacity data for a ternary gas mixture of CO₂, CH₄ and N₂ as well as pure and binary gas mixtures of the same components on a commercial zeolite 13X, measured at temperatures of (273, 303 and 333 K) and pressures from (25 to 900 kPa) using a dynamic column breakthrough (DCB) apparatus. Although previous adsorption studies have reported the adsorption equilibria of pure and to a lesser degree binary gas mixtures on zeolite 13X, no experimental data are available in the literature for a ternary gas mixture of CO₂, CH₄ and N₂ on zeolite 13X APG-III, a promising adsorbent for carbon capture and natural gas separation. The measured pure component adsorption capacities were regressed to a Toth isotherm model and the obtained Toth parameters were used to implement an IAST model for binary and ternary adsorption predictions. The IAST predictions of mixture gas adsorption represented the binary and ternary adsorption equilibria well with their corresponding maximum deviations being 0.055 and 0.3 mmol/g, respectively. This indicates the IAST can be applied successfully to these adsorption systems even though they involve molecules with different adsorption affinity and adsorbents with heterogeneous surfaces.

Keywords Carbon dioxide · Zeolite 13X APG-III · Ternary adsorption · Dynamic column breakthrough · IAST

1 Introduction

The separation of CO₂ and N₂ from CH₄ containing gas mixtures is an essential step in many industrial applications such as upgrading wellhead natural gas to pipeline gas specifications (Watson et al. 2011), ensuring the safe production and storage of liquefied natural gas (LNG) (Kidnay et al. 2011), and promoting the commercialisation of sub-quality reservoirs that comprise a significant portion of the reserves

world-wide (Rufford et al. 2012). In recent years, pressure swing adsorption (PSA) technology has attracted much attention for the separation of CO₂ and N₂ from CH₄ due to its potential in lowering the separation cost (Rufford et al. 2012; Saleman et al. 2017; Xiao et al. 2016).

For a PSA separation, the mixture gas adsorption equilibrium data are essential to the design and simulation of the process. However, there are limited literature data for experimental mixture gas adsorption equilibrium because the measurement of such data is still one of the most challenging experiments in adsorption research (Walton and Sholl 2015). Instead, multicomponent adsorption data used for design or simulation are often predictions from various models based only on pure component adsorption experiments. The ideal adsorbed solution theory (IAST) developed by Myers and Prausnitz (1965) is the most widely used and a generally reliable method for predicting mixture adsorption using only pure component adsorption isotherms (Walton

Electronic supplementary material The online version of this article (<https://doi.org/10.1007/s10450-018-9952-3>) contains supplementary material, which is available to authorized users.

✉ Eric F. May
Eric.May@uwa.edu.au

¹ Fluid Science & Resources Division, Department of Chemical Engineering, The University of Western Australia, 35 Stirling Highway, Perth, WA 6009, Australia

and Sholl 2015). The fundamental assumption of the IAST theory is that the adsorbed phase is an ideal solution which requires adsorbed molecules to have similar affinities for the adsorbent (Talu 2013; Myers and Monson 2014). Therefore, it is generally thought that the IAST will produce large deviations between prediction and experimental data for mixtures containing molecules with significant variations in polarity and adsorption affinity, and for adsorbents, such as zeolites, involving heterogeneous surfaces (Walton and Sholl 2015). Such deviations of prediction from reality lead to unnecessary uncertainties in the design and simulation of adsorption processes.

In fact, multicomponent adsorption equilibria can be quickly and reliably measured using a dynamic column breakthrough (DCB) apparatus such as the one described by Hofman et al. (2012) and Saleman et al. (2013). In this technique, adsorbate gases flow, in known ratios, through a column packed with an adsorbent material. Through the knowledge of the gas feed flow rate and composition, adsorption column pressure and temperature, and effluent composition and flow rate, the amount of gas accumulated in the column can be calculated, from which the equilibrium adsorption capacity can be determined (Saleman et al. 2013; Delgado et al. 2006, 2007; Rufford et al. 2013). An advantage of the dynamic breakthrough technique is that this method is inherently capable of measuring adsorption equilibria for gas mixtures without any modifications or additional assumptions in the analysis; this allows rapid characterisation of adsorption isotherms over a wide range of temperatures and pressures, including sub-ambient pressures through dilution of the adsorbate with an inert gas.

In this work, the dynamic column breakthrough technique was used to measure the adsorption equilibria of pure, binary and ternary mixtures of CO₂, N₂ and CH₄ on zeolite 13X APG-III which is a commercially available adsorbent developed for the removal of CO₂ in cryogenic O₂ plants and studied for the removal of CO₂ from flue gases using pressure swing adsorption processes (Xiao et al. 2012). Results for this particular adsorbent have not been reported for natural gas separations although data for other forms of zeolite 13X have been measured in the context of separating CO₂ and N₂ from natural gas (Wang 2012a; b; Cavonati et al. 2004, 2006). Given the higher CO₂ capacity of zeolite 13X APG-III than other versions of zeolite 13X, it might as well be used for the separation of CO₂ and N₂ from natural gas. Therefore, its adsorption capacity for N₂, CH₄ and CO₂, especially for binary and ternary mixtures, needs to be understood to assess the performance of APG-III for adsorption processes. Thus, the adsorption equilibria of pure, binary and ternary mixtures were measured at temperatures from (273 to 333 K) and pressures from (25 to 900 kPa). The pure gas equilibrium data were represented with the Toth isotherm model and the binary and ternary

equilibrium data were compared with the IAST predictions to examine the ability of this model to represent this system.

2 Experimental section

2.1 Materials

Commercial zeolite 13X, UOP MOLSIV™ APG-III, was used in this study. This adsorbent was provided in the form of spherical beads with an average particle diameter of 1.9 mm and a BET surface area of 546 m²/g measured with nitrogen at 77 K. The skeletal density of the adsorbent was 2346 kg m⁻³ measured using a helium Pycnometer. All gases used in this work were supplied by BOC (Australia) with the following stated mole fraction purities: He—99.999%, CH₄—99.995%, CO₂—99.995% and N₂—99.999%.

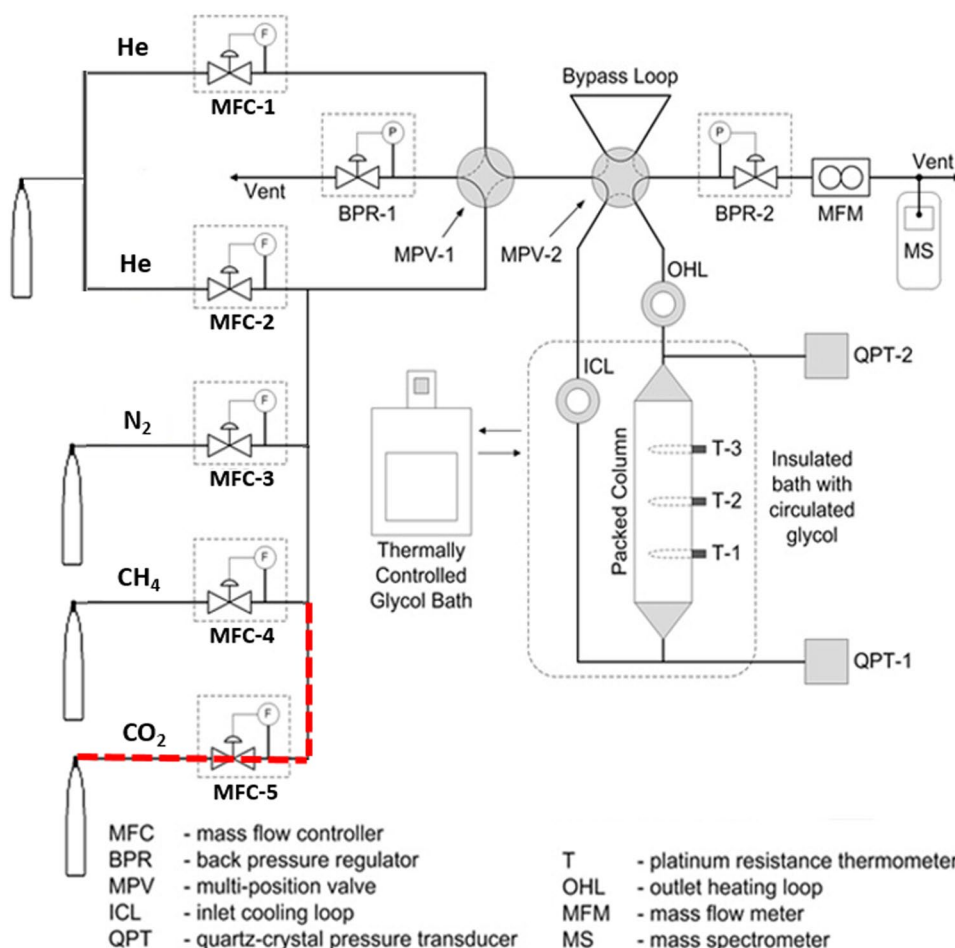
2.2 Apparatus and procedure

Pure gas and binary gas mixture adsorption equilibrium capacities were all measured using the same dynamic column breakthrough apparatus and procedure reported previously (Saleman et al. 2013, 2017; Hofman et al. 2012). Ternary gas mixture adsorption data were measured using the same apparatus but modified with an additional gas inlet line as indicated by the red dashed line in Fig. 1. The cylindrical stainless steel adsorption column, with a length of 130 mm and an internal diameter of 22.2 mm, was packed with 31.761 g of activated zeolite 13X APG-III beads. The activation of the adsorbent was carried out stepwise in a vacuum autoclave: the adsorbent was first heated to 120 °C and held at this temperature under vacuum for 2 h; then the temperature was increased to 200 °C and kept at 200 °C for 1 h before the temperature was increased to 350 °C and where it was held for at least 8 h. The adsorbent was then cooled down to about 30–40 °C, and the vacuum autoclave was filled with helium to about 1 atm pressure. After the adsorbent was packed into the adsorption column, the column was flushed with helium at room temperature until the connected outlet gas analyser reached a helium mole fraction of 1.00 after which gas adsorption measurements were commenced. Pure N₂, CH₄, CO₂ isotherms and their binary and ternary mixtures were measured over the pressure range of (25–900 kPa) at temperatures of 273, 303 and 333 K.

2.3 Interpretation of adsorption data

The equilibrium adsorption capacities of gases on the adsorbent were derived via a mass balance analysis of gases entering/leaving and accumulated in the adsorption column (Saleman et al. 2013, 2017). The amount of gas flowing into and out of the adsorption column can be obtained by integrating

Fig. 1 The process flow schematic diagram of the dynamic column breakthrough apparatus (Saleman et al. 2017). (Color figure online)



the mass flow readings of each component gas before and after the adsorption column. The amount of gas accumulated in the adsorption column comprises gas adsorbed on the adsorbent and gas in the void volume of the bed which was measured through the displacement of helium. Therefore, this dynamic column breakthrough method measures excess adsorption capacities because the volume of helium displaced from the column is assumed to be the volume of gas in equilibrium with the adsorbed phase on the adsorbent at the end of each experiment. However, this assumption ignores the volume of the adsorbed phase which is not present when the adsorption column is filled with pure helium. The absolute adsorption capacities were then calculated from the measured excess capacities and adsorbed phase densities using Eq. 1 (Watson et al. 2009).

$$Q_{abs} = \frac{Q_{ex}}{1 - \rho_{M,gas}/\rho_{M,ads}} \tag{1}$$

Here Q_{abs} is the absolute adsorption capacity, Q_{ex} is the excess adsorption capacity, $\rho_{M,gas}$ and $\rho_{M,ads}$ are the mass densities of the gas phase and adsorbed phase, respectively.

The mass densities of the pure gas and mixture gases at various temperature, pressure and compositions were obtained from the software package REFPROP 9.1 (NIST 2013). For pure fluids, literature values of the adsorbed phase densities for pure compounds ($\rho_{ads,CO_2} = 1.170 \text{ g}\cdot\text{cm}^{-3}$, $\rho_{ads,CH_4} = 0.354 \text{ g}\cdot\text{cm}^{-3}$ and $\rho_{ads,N_2} = 0.701 \text{ g}\cdot\text{cm}^{-3}$) (Watson et al. 2009; Hefti et al. 2015; Sudibandriyo et al. 2003) were used. These adsorbed phase densities were obtained using the Ono–Kondo model and assumed to be independent of pressure and temperature as pointed out by Watson et al. (2009), who also found the uncertainty in calculated densities could vary by about 10% using different methods (Sudibandriyo et al. 2003) such as Ono–Kondo, ZGR EOS, VDM covolume. For mixture gases, an ideal mixing rule was used to estimate the adsorbed phase densities. Detailed analyses of how reliable equilibrium adsorption capacities can be determined with this apparatus are provided by Hoffman et al. (2012) and Saleman et al. (2013). For brevity and convenience of discussion, the absolute adsorption capacity, Q_{abs} , is referred as Q in equations, figures and tables in the following sections.

2.4 Measurement uncertainties

The contributing sources of measurement uncertainty in the adsorption capacities are listed in Table 1 and are as reported by Hofman et al. (2012). They identified that the most significant uncertainty source was the measurement of the difference between the flow rates entering and exiting the column. Quantification of the overall adsorption capacity measurement uncertainties can thus be achieved from the uncertainties in the total molar flow measurements for pure component measurements (Eq. 2) and the component molar flows for measurements with multicomponent mixtures (Eq. 3).

$$\frac{u(Q)}{Q} \cong \frac{\sqrt{u(f)^2 + u(F)^2}}{f - F} \quad (\text{For pure fluids}) \quad (2)$$

Here f is the inflow, F is the average effluent flow rate from time $t=0$ up to shortly after reaching steady-state and $u(x)$ indicates the uncertainty in the quantity x .

$$\frac{u(Q_j)}{Q} \cong \frac{\sqrt{u(f_j)^2 + u(F_j)^2 + u(y_j * F_{He})^2}}{f_j - F_j - y_j * F_{He}} \quad (\text{For multicomponent mixtures}) \quad (3)$$

Here $F_j = y_j F$ is the molar flow of each component. The uncertainty is estimated for each component and displayed as an error bar in each of the result plots.

3 Model description

3.1 Toth model

The Toth model was used to regress the pure component adsorption data. The Toth isotherm equation is recommended for microporous adsorbents and has been used extensively for adsorption data representation and adsorption process simulations (Valenzuela and Myers 1989). The expression of the Toth model is shown in Eq. 4.

$$Q_{abs} = Q_{max} \frac{KP}{[(1 + (KP)^n)]^{1/n}}; K = K_0 \exp\left(\frac{-\Delta H}{RT}\right) \quad (4)$$

where Q_{max} , K_0 , ΔH , n are adjustable empirical parameters, where n is the adsorbent heterogeneity factor, ΔH is the enthalpy of adsorption, Q_{max} is maximum equilibrium adsorption capacity and K_0 is the equilibrium parameter at infinite temperature. The other standard parameters in the equation are R and T which are the ideal gas constant and the gas temperature, respectively.

3.2 Ideal adsorbed solution theory (IAST)

The ideal adsorption solution theory (IAST) proposed by Myers and Prausnitz is a thermodynamically consistent approach to predicting multicomponent adsorption equilibria based on pure component isotherms (Myers and Prausnitz 1965). This theory was developed with an assumption among others that the spreading pressures of the components must be equal at constant temperature, where the spreading pressure (π) for a single component can be calculated from the Gibbs adsorption isotherm as follows (Thomas and Crittenden 1998):

$$\pi = RT \int_0^{p_i^0} \left(\frac{n_i^0}{A}\right) d \ln P \quad (5)$$

Thus, the condition $\pi_{mix} = \pi_i = \pi_j = \dots = \pi_N$ must be fulfilled to meet the IAST requirement for a mixture composed of N (number of species in the mixture) components, which leads to the following expression:

$$\pi A / RT = \int_0^{p_i^0} \frac{n_i^0}{p_i} dp_i = \int_0^{p_j^0} \frac{n_j^0}{p_j} dp_j = \dots = \int_0^{p_N^0} \frac{n_N^0}{p_N} dp_N \quad (6)$$

where p_i^0 is the hypothetical equilibrium gas phase pressure exerted by the respective pure component i , over area A , when it has the same temperature and spreading pressure (π_{mix}) of the adsorbed phase in a mixture system, n_i^0 is the corresponding capacity for the pure component i , and p_i is

Table 1 Component uncertainties associated with DCB apparatus (Hofman et al. 2012)

Component	Uncertainty
Mass flow meter (MFM)	1.6% of reading + 0.2% of full scale
Mass flow controller (MFC)	0.8% of reading + 0.2% of full scale
Back pressure regulator (BPR)	0.25% of full scale
Quartz-crystal pressure transducer (QPT)	0.1 kPa
Mass spectrometer (MS)	0.01 mol fraction
Platinum resistance thermometer (PRT)	0.2 K
Mass of adsorbent	5 mg

the gas phase pressure exerted by component i in the mixture, which can be expressed as $p_i = p_i^0(\pi)x_i$ with x_i being the mole fraction of i in the adsorbed phase.

The p_i can also be expressed as $p_i = y_iP$ if the total pressure of the mixture is P and the mole fraction of i in the vapour phase is y_i . Therefore, at equilibrium conditions for a component i in a multicomponent mixture, the following equation can be obtained

$$y_iP = p_i^0(\pi)x_i \tag{7}$$

Assuming the total pressure P and mole fraction y_i of component i in the vapour phase are known, then the calculation procedure for a mixture involves finding p_i^0 and x_i by solving Eqs. 6 and 7 simultaneously subject to the constraint $\sum x_i = 1$. Once values of p_i^0 have been found, n_i^0 can be calculated and with the x_i values also known, the total adsorbed amount, n_T , can be calculated using standard state loadings from the pure component isotherms

$$\frac{1}{n_T} = \sum_{i=1}^N \frac{x_i}{n_i^0} \tag{8}$$

The adsorption of each species in the mixture is then calculated by

$$n_i = x_i n_T \tag{9}$$

4 Results and discussion

4.1 Pure component equilibria

Pure component adsorption data for N_2 , CH_4 and CO_2 on zeolite 13X APG-III in the pressure range of 25–900 kPa at three temperatures (273, 303 and 333 K) are shown in Fig. 2. The corresponding optimal regression plots using the Toth isotherm model are also shown in the figure. The deviations of the experimental data from the predicted values as a fraction of the measured data are shown in Fig. 3. The Toth model parameters determined by regression with their associated statistical uncertainties are presented in Table 2. As seen from the plots, the pure gas adsorption data could be well represented by the Toth isotherm model, with a standard deviation of 0.004 mmol/g for N_2 , 0.004 mmol/g for CH_4 and 0.02 mmol/g for CO_2 , which are all within the experimental uncertainties for these measurements. In addition, all the Toth model parameters were obtained with small statistical uncertainties except for the K_0 parameter for CO_2 , for which the uncertainty was larger than the parameter value; this was caused by the fact that there were fewer measurements made in the low pressure range to adequately cover the large variation in the adsorption capacity of CO_2 that occurs for a relatively small change in pressure.

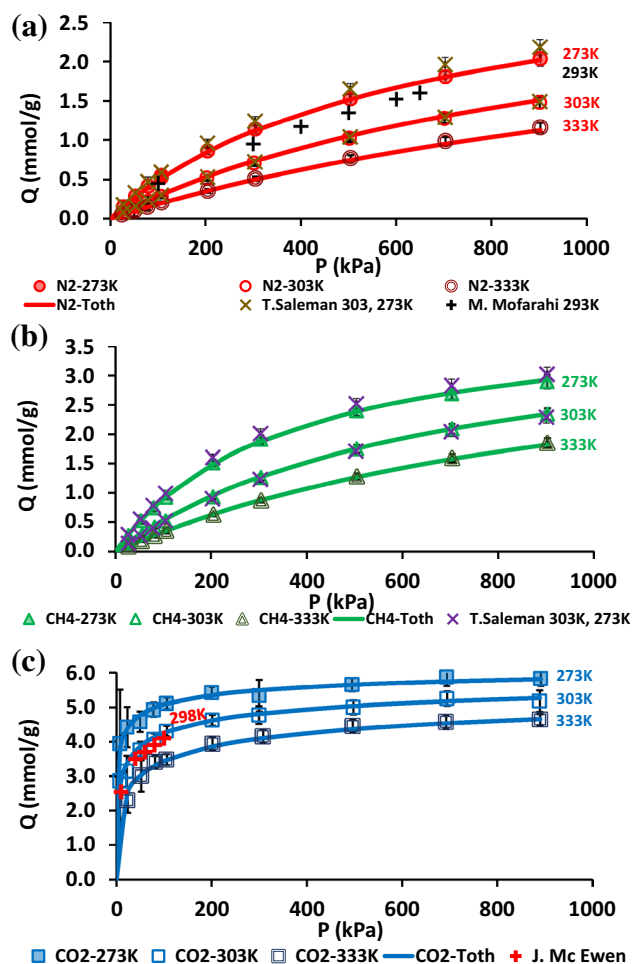


Fig. 2 Experimental data and regressed Toth isotherms for a N_2 , b CH_4 and, c CO_2

The equilibrium adsorption amount of each component increased with pressure at constant temperature; however, the initial increase of CO_2 adsorption at low pressure (< 100 kPa) region was more prominent than the increases for N_2 and CH_4 . At all temperatures, the measured equilibrium capacity of CO_2 was higher than that of N_2 and CH_4 for the same pressure because of the stronger polarizability of CO_2 compared to CH_4 and N_2 (Mulgundmath et al. 2012). For N_2 , the maximum adsorption capacity measured at 273 K was 2.03 mmol/g at a pressure of 902 kPa, and capacities with the same pressure at 303 and 333 K were 1.48 and 1.16 mmol/g, respectively. For CH_4 , the maximum adsorption capacity measured at 273 K was 2.9 mmol/g at a pressure of 903 kPa, and the corresponding capacities for the same pressure at 303 and 333 K were 2.34 and 1.85 mmol/g, respectively. For CO_2 , the maximum adsorption capacity measured at 273 K was 5.83 mmol/g at a pressure of 891 kPa, and the corresponding capacities for the same pressure at 303 and 333 K were 5.18 and 4.65 mmol/g,

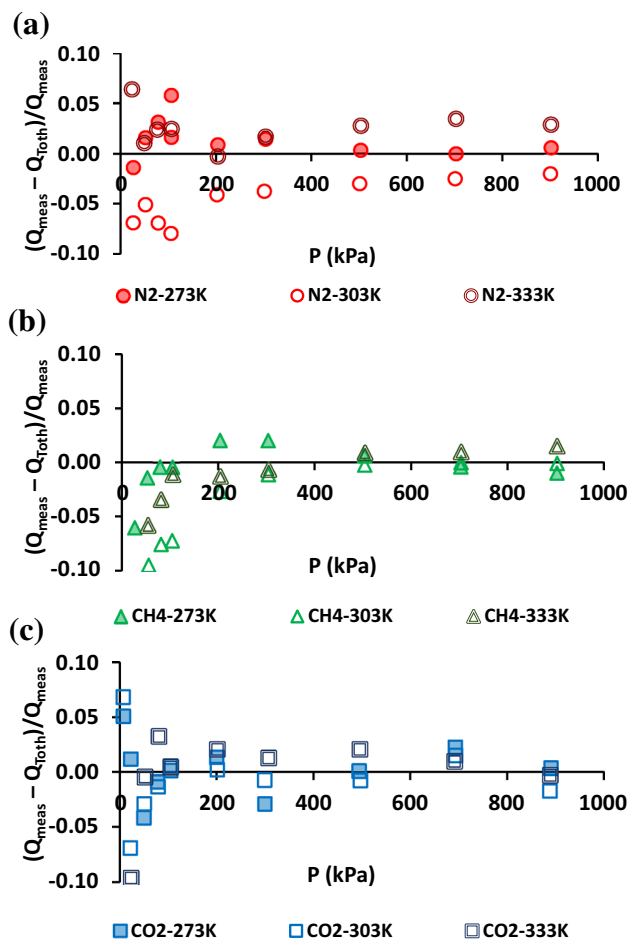


Fig. 3 Relative deviation plots of pure component experimental data from regressed Toth models: **a** N₂, **b** CH₄ and **c** CO₂

Table 2 Toth isotherm parameters regressed to data measured across three isotherms (273, 303 and 333 K)

	CH ₄	N ₂	CO ₂
Data points (N)	27	29	29
Q_{\max} (mmol/g)	4.11 ± 0.15	3.85 ± 0.82	6.82 ± 0.73
$K_0 \times 10^6$ (1/kPa)	4.99 ± 0.09	3.89 ± 0.95	1.29 ± 2.78
$-\Delta H$ (kJ/mol)	14.4 ± 0.5	13.6 ± 0.5	39.2 ± 4.0
n	0.99 ± 0.11	0.86 ± 0.16	0.29 ± 0.08
RMSD (mmol/g)	0.004	0.004	0.020

respectively. The experimental data were found to be consistent with existing literature data (Wang 2012; Cavenati et al. 2004, 2006).

Following a review of the published data on Zeolite 13X, three additional recent data sets measured under relatively similar experimental conditions have been plotted for comparison. These data are from Mofarahi and Shokroo (2013) (N₂), McEwan et al. (2013) (CO₂), and Saleman et al. (2017)

(CH₄ and N₂). The published data are in very good agreement with the present measurements.

4.2 Binary gas mixture adsorption equilibria

Binary adsorption equilibria were measured for three different binary gas mixtures, namely CO₂ + N₂, CO₂ + CH₄ and CH₄ + N₂. The experiments were conducted over three temperatures (273, 303 and 333 K), each with two overall system pressures (100 and 900 kPa), incorporating three combinations of mixture composition (25/75%, 50/50% and 75/25%). This resulted in 18 experiments for each binary mixture and a total of 54 binary experiments which are tabulated in Tables 3, 4 and 5. To check the thermodynamic consistency of the pure gas results with the binary adsorption data and the internal consistency of the binary data, consistency tests were carried out for each of the three pairs (CO₂ + N₂, CO₂ + CH₄, and CH₄ + N₂) of binary experiments using the data obtained at the temperature of 273 K with the method suggested by Sircar et al. (Rao and Sircar 1999). A brief introduction of the equations used for the consistency tests and the results of comparison are given in the Supporting Information. These binary experimental data are also plotted in Fig. 4 (CO₂ + CH₄ and CO₂ + N₂) and Fig. 6 (CH₄ + N₂) along with adsorption predictions from the IAST implemented using the algorithm of Valenzuela and Myers (1989), with Toth isotherm parameters obtained from the pure component adsorption equilibria. It can be seen that the affinity of CO₂ towards Zeolite 13X is much higher than those of CH₄ and N₂. This translates to a non-uniform site energy distribution for binary mixtures containing CO₂, which can be represented by a quasi-IAST isotherm for the mixture based on the Toth function (Kumar et al. 2011). For CO₂ at partial pressures above 10 kPa, the adsorption on Zeolite 13X can be represented within experimental uncertainty from the partial pressure alone using the quasi-IAST isotherm. The deviations between the experimental data and the predictions from the IAST model as a percentage of the experimental values are shown in Fig. 5 (CO₂ + CH₄ and CO₂ + N₂) and Fig. 7 (CH₄ + N₂). Zeolite 13X has an extremely strong affinity towards CO₂ compared to CH₄ or N₂ as can be seen in the values of equilibrium selectivity shown in Tables 3 and 4. Selectivity was calculated based on the following formula for carbon dioxide over methane:

$$\alpha_{CO_2-CH_4} = \frac{Q_{CO_2}/y_{CO_2}}{Q_{CH_4}/y_{CH_4}} \quad (10)$$

Similar equations were used to evaluate the selectivity of CO₂ over N₂ (Table 4) and CH₄ over N₂ (Table 5). Figure 6 shows the adsorption observed for the CH₄ + N₂ binary mixture, with Fig. 7 showing the deviations of those data from the predictions of the IAST. The values of $\alpha_{CH_4-N_2}$

Table 3 CH₄ + CO₂ binary mixture adsorption capacity data

T (K)	P (kPa)	CH ₄			CO ₂			Selectivity	
		y _i (mol/mol)	Q (mmol/g)	u(Q) (mmol/g)	y _i (mol/mol)	Q (mmol/g)	u(Q) (mmol/g)	(α _{CO₂-CH₄}) _{meas}	(α _{CO₂-CH₄}) _{IAST}
333	106	0.76	0.25	0.11	0.24	2.43	0.24	32	137
	106	0.52	0.20	0.07	0.48	3.01	0.14	17	122
	106	0.26	0.04	0.02	0.74	3.44	0.10	32	116
	903	0.80	0.39	0.09	0.20	3.71	0.43	37	109
	903	0.56	0.22	0.04	0.44	4.38	0.24	25	111
	903	0.31	0.10	0.02	0.69	4.58	0.16	20	115
303	113	0.76	0.31	0.12	0.24	3.38	0.32	35	198
	107	0.52	0.18	0.05	0.48	3.91	0.18	23	195
	107	0.26	0.05	0.02	0.74	4.16	0.12	27	196
	902	0.79	0.32	0.07	0.21	4.33	0.49	51	212
	902	0.56	0.30	0.04	0.44	4.90	0.26	20	240
	902	0.31	0.14	0.02	0.69	5.07	0.18	16	266
273	106	0.76	0.32	0.11	0.24	4.22	0.40	42	305
	106	0.51	0.21	0.05	0.49	4.77	0.21	23	338
	106	0.26	0.05	0.01	0.74	4.99	0.15	35	367
	903	0.79	0.46	0.09	0.21	5.08	0.57	42	460
	903	0.55	0.17	0.02	0.45	5.65	0.30	39	593
	903	0.31	0.16	0.03	0.69	6.03	0.21	17	695

Table 4 N₂ + CO₂ binary mixture adsorption capacity data

T (K)	P (kPa)	N ₂			CO ₂			Selectivity	
		y _i (mol/mol)	Q (mmol/g)	u(Q) (mmol/g)	y _i (mol/mol)	Q (mmol/g)	u(Q) (mmol/g)	(α _{CO₂-N₂}) _{meas}	(α _{CO₂-N₂}) _{IAST}
333	108	0.75	0	0.08	0.25	2.71	0.25	*	309
	108	0.49	0	0.36	0.51	3.42	0.15	*	290
	107	0.25	0	0.44	0.75	3.69	0.11	*	284
	902	0.79	0	0.05	0.21	3.97	0.46	*	286
	902	0.54	0	0.07	0.46	4.40	0.24	*	309
	902	0.28	0	0.06	0.72	4.73	0.16	*	332
303	107	0.75	0	0.02	0.25	3.49	0.32	*	499
	107	0.48	0	0.42	0.52	4.13	0.18	*	517
	106	0.24	0	0.21	0.76	4.35	0.13	*	537
	902	0.78	0.01	0.00	0.22	4.74	0.53	2330	624
	901	0.52	0.01	0.03	0.48	5.23	0.27	769	765
	902	0.28	0	0.05	0.72	5.29	0.18	*	873
273	107	0.75	0	0.07	0.25	4.47	0.41	*	867
	108	0.48	0	0.19	0.52	5.07	0.22	*	1027
	108	0.24	0	0.26	0.76	5.24	0.15	*	1148
	903	0.78	0.02	0.02	0.22	5.35	0.59	962	1559
	902	0.52	0.01	0.08	0.48	5.93	0.30	644	2176
	902	0.28	0	0.09	0.72	6.03	0.21	*	2639

Cells with * denote instances when the selectivity calculation was not done given that the measured equilibrium adsorption capacity for nitrogen was very small and comparable with the experimental uncertainty

shown in Table 5 are similar with the literature values for other common adsorbents such as activated carbon (Rufford et al. 2013).

From Figs. 5 and 7, it can be seen that the IAST could provide accurate predictions of the equilibrium capacities for the binary mixture components. The root mean square

Table 5 CH₄+N₂ binary mixture adsorption capacity data

T (K)	P (kPa)	CH ₄			N ₂			Selectivity ($\alpha_{\text{CH}_4\text{-N}_2}$) _{meas}
		y _i (mol/mol)	Q (mmol/g)	u(Q) (mmol/g)	y _i (mol/mol)	Q (mmol/g)	u(Q) (mmol/g)	
333	105	0.74	0.27	0.02	0.26	0.05	0.02	1.8
	106	0.51	0.18	0.01	0.49	0.10	0.01	1.8
	106	0.27	0.10	0.01	0.73	0.15	0.02	1.8
	902	0.76	1.46	0.07	0.24	0.25	0.07	1.9
	902	0.53	1.08	0.07	0.47	0.47	0.07	2.0
	902	0.30	0.63	0.07	0.70	0.75	0.07	2.0
303	106	0.74	0.39	0.02	0.26	0.08	0.02	1.6
	106	0.50	0.27	0.02	0.50	0.15	0.02	1.8
	106	0.26	0.14	0.02	0.74	0.23	0.02	1.8
	902	0.76	1.70	0.09	0.24	0.25	0.08	2.1
	902	0.53	1.44	0.10	0.47	0.61	0.09	2.1
	901	0.30	0.86	0.09	0.70	0.98	0.09	2.1
273	106	0.74	0.68	0.03	0.26	0.13	0.03	1.9
	107	0.50	0.48	0.03	0.50	0.24	0.03	1.9
	107	0.26	0.25	0.03	0.74	0.37	0.03	1.9
	902	0.76	2.31	0.12	0.24	0.34	0.09	2.2
	902	0.53	1.83	0.13	0.47	0.73	0.11	2.2
	902	0.30	1.12	0.12	0.70	1.19	0.11	2.3

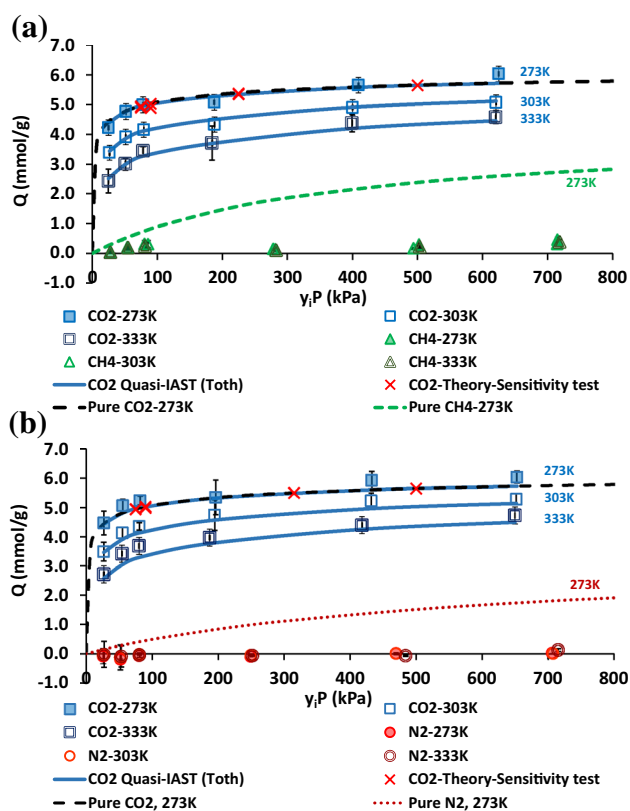


Fig. 4 Adsorption capacity and IAST (Toth) prediction at 333, 303 and 273 K for **a** CO₂+CH₄ and **b** CO₂+N₂ binary gas mixture. IAST predictions for CH₄ and N₂ in their binary mixtures with CO₂ are not shown due to the negligible amount of adsorption

deviation between the IAST predictions and the measured equilibrium adsorption capacities were 0.030 mmol/g for CO₂ and 0.048 mmol/g for CH₄ for the CO₂+CH₄ mixture, 0.055 mmol/g for CO₂ and 0.020 mmol/g for N₂ for the CO₂+N₂ mixture, and 0.003 mmol/g for CH₄ and 0.014 mmol/g for N₂ for the CH₄+N₂ mixture, which were all less than the measurement uncertainties. Figure 4 also shows the competitive adsorption among CO₂, CH₄ and N₂. The presence of CO₂ reduced the CH₄ adsorption capacity by 98% in the binary gas mixtures of CO₂+CH₄ (Fig. 4a) compared to pure CH₄ adsorption, and the N₂ adsorption capacity by 99% in the binary gas mixtures of CO₂+N₂ (Figs. 4, 6b) compared to pure N₂ adsorption. In binary mixtures of CH₄+N₂ (Fig. 6), both gases exhibited more adsorption on zeolite 13X than in mixtures containing CO₂; however, a reduction in adsorption capacity was observed for both gases (N₂ by 32% and CH₄ by ~10%) when compared to their pure fluid adsorption capacities.

In these experiments, both the feed composition (25–80%) and the total system pressure (1–9 bar) were varied for all binary gas mixtures to study the effect of gas composition on the competitive adsorption of gases at different total pressures. This is useful for verifying the performance of predictive models for competitive adsorption used to simulate dynamic PSA processes since both the total pressure and gas compositions frequently change during a cycle. It is commonly expected that at constant temperature the adsorption amount of a gas in a mixture will vary with changes in either the gas composition or the

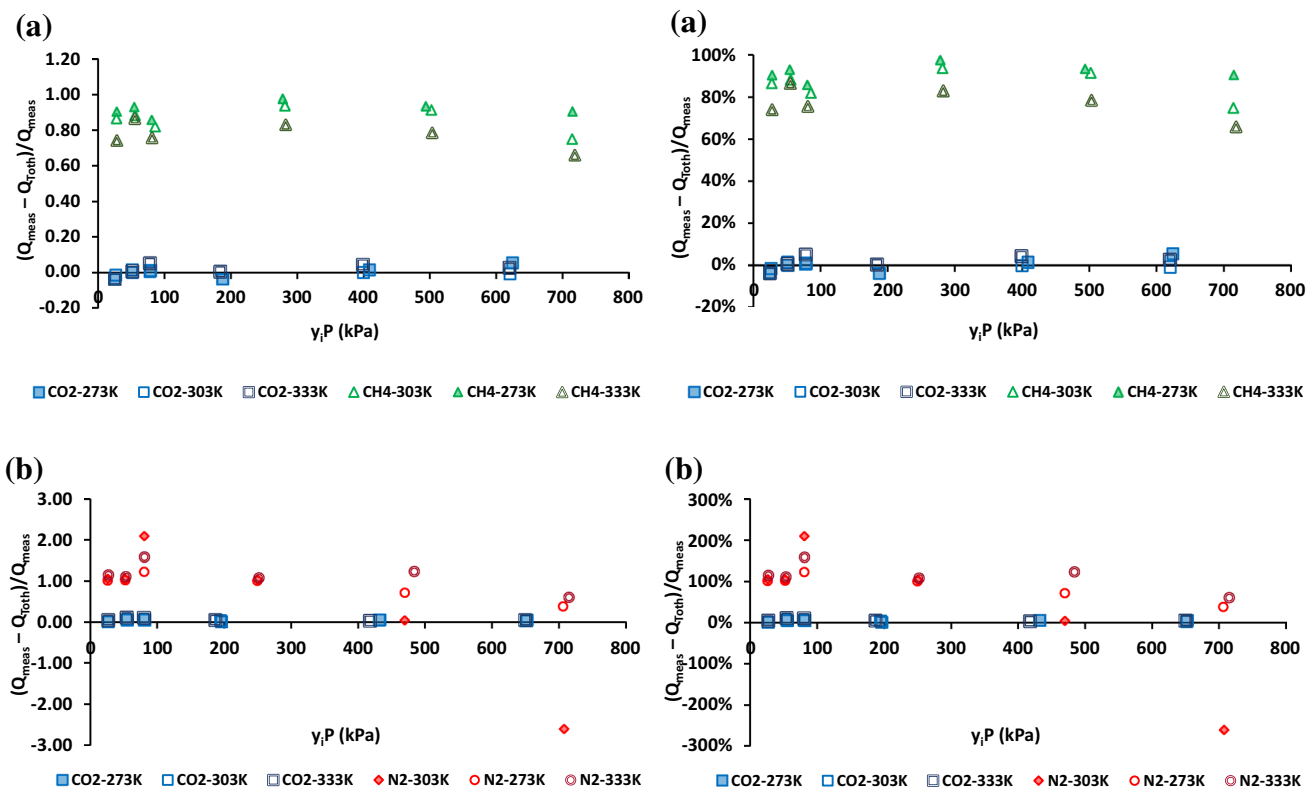


Fig. 5 Deviation plots of CO₂ experimental data from IAST (Toth) model as a % of experimental data at 333, 303 and 273K for **a** (CO₂+CH₄) and **b** (CO₂+N₂) binary gas mixtures. Deviation

data for CH₄ and N₂ are not plotted due to the negligible amount of adsorption measured in the presence of CO₂

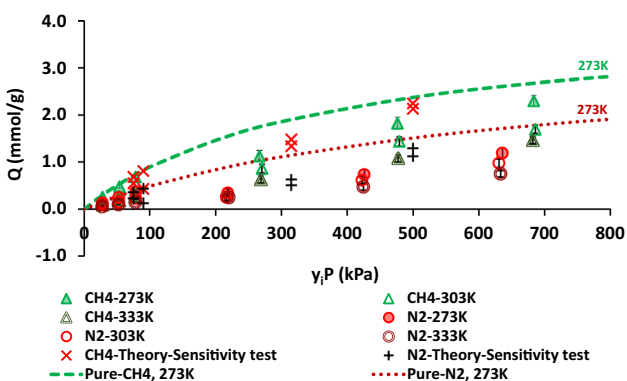


Fig. 6 Adsorption Capacity at 333, 303 and 273 K for CH₄+N₂ binary gas mixture, showing pure component isotherm data as dashed lines

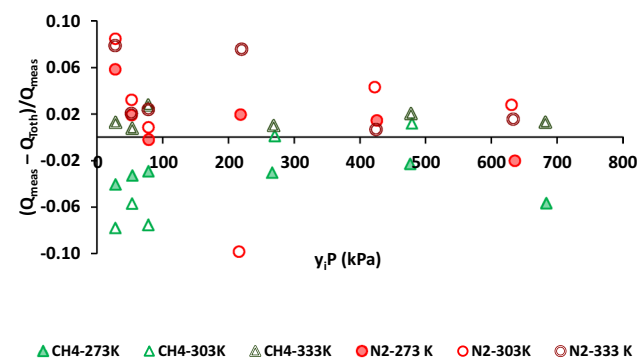


Fig. 7 Deviation plot of experimental data from IAST (Toth) model as a % of experimental data at 333, 303 and 273 K for (CH₄+N₂)

total system pressure because of competitive adsorption, even if the partial pressure of each adsorbate is held the same. However, the extent of any reduction depends on the relative affinities of the adsorbates in competition; potentially, the adsorption of higher affinity gas will only be slightly lessened by the presence of the weakly adsorbed gas. As an example, the adsorption of CO₂ at a partial

pressure of 25 kPa in a binary mixture of CO₂ and CH₄ at a total pressure of either 100 or 400 kPa was measured at 273 K. The decrease in CO₂ adsorption resulting from an increase in total pressure from 100 to 400 kPa was only 3.8% despite the significant reduction in CO₂ fraction from 25 to 6.25 mol%. For the CO₂ and N₂ mixture, the impact of such changes were even smaller with a reduction in CO₂ adsorption at constant partial pressure of only 1.5%. In contrast, the four-fold reduction in CO₂ mole fraction

and four-fold increase in system pressure resulted in an increase the adsorption of both CH_4 and N_2 by a factor of about 3.8.

The spreading pressures extrapolated during the IAST calculations for CH_4 in binary mixture of $\text{CH}_4\text{--CO}_2$ was $\sim 13,000$ kPa, whilst the corresponding spreading pressure for N_2 in a $\text{N}_2\text{--CO}_2$ mixture was $\sim 15,000$ kPa. These exceedingly high spreading pressures were not covered by the pure component isotherm measurements and are thus a concern for the validity of using IAST to predict mixture gas adsorption. However, the reasonable agreement between the binary data and the IAST model in this work showed that the extrapolation of spreading pressure did not affect the predictive capability of the IAST model.

4.3 Ternary experiments with CO_2 , N_2 & CH_4 gas mixture

The ternary adsorption equilibria were measured for ternary mixtures of $\text{N}_2 + \text{CH}_4 + \text{CO}_2$ prepared by flow, where the ratio of $\text{N}_2\text{--CH}_4$ was always approximately 1:1, while the approximate CO_2 mole fraction was either 0.8, 0.6 or 0.4. These experiments were conducted at three temperature (273, 303 and 333 K) and three overall system pressures around (100, 500 and 900 kPa). The results of these 27 ternary experiments with measurement uncertainties are listed in Table 6 and plotted in Fig. 8 along with the regressed Toth model for pure CO_2 at the corresponding temperatures/partial pressures and IAST predictions for the mixtures based on pure component Toth model parameters.

Comparison of equilibrium adsorption amounts in the ternary mixtures with those predicted for the pure gas adsorption isotherms (Fig. 8) reveals that the CO_2 equilibrium adsorption capacity was not affected by the presence of either methane or nitrogen in a ternary gas mixture while in contrast the CH_4 and N_2 adsorption amounts were significantly suppressed in the mixture. To be specific, an exemplar comparison is made for the adsorption at a temperature of 273 K and a total pressure of 902 kPa. At the equivalent partial pressure of 250 kPa, the adsorption capacity of N_2 was reduced from 1.12 mmol/g for the pure gas to 0.02 mmol/g in a ternary mixture of 28% $\text{N}_2 + 37\%$ $\text{CH}_4 + 35\%$ CO_2 . Similarly the adsorption capacity of CH_4 at this partial

pressure was reduced from 1.87 mmol/g for the pure gas to 0.13 mmol/g in a ternary mixture of 18% $\text{N}_2 + 27\%$ $\text{CH}_4 + 55\%$ CO_2 as shown in Fig. 8. In contrast, the sorption of CO_2 in the mixture at a partial pressure of ~ 500 kPa in the ternary gas mixture of 28% $\text{N}_2 + 18\%$ $\text{CH}_4 + 55\%$ CO_2 was the same within the measurement uncertainty as its adsorption capacity for the pure fluid at the same partial pressure at 5.7 mmol/g. Figure 9 shows a deviation plot for the difference between the measured data and the IAST (Toth) model predictions as a percentage of the measured data. The data confirm that the IAST (Toth) model predicts the measured CO_2 sorption values with reasonable accuracy and is therefore a representative model for the ternary gas mixture data. The deviations for CH_4 and N_2 are not plotted due to the negligible measured adsorption in the presence of CO_2 .

5 Conclusion

Knowledge of mixture gas adsorption equilibrium data is critical to the design and simulation of adsorption based processes. In this paper adsorption data of pure CO_2 , CH_4 and N_2 on zeolite 13X APG-III were measured at different pressures in the range of 25–900 kPa and three different temperatures (273, 303 and 333 K). The CO_2 adsorption amount was much higher than that of N_2 and CH_4 at the conditions measured. The pure gas adsorption data could be well described using a Toth isotherm model with parameters obtained by regression of the data. Experimental binary and ternary adsorption equilibria data were also measured for mixtures of CO_2 , CH_4 and N_2 in the same temperature and pressure range, and compared to IAST predictions based on the Toth model parameters determined from the pure gas adsorption data. The IAST predictions of mixture gas adsorption could represent the binary and ternary adsorption equilibria well with corresponding maximum deviations being 0.055 and 0.3 mmol/g, respectively, indicating the IAST predictions of CO_2 , CH_4 and N_2 mixture gas adsorption on zeolite 13X are robust and that the IAST can be reliably used for process design calculations using this adsorbent.

Table 6 Ternary mixture adsorption capacity data

T (K)	P (kPa)	CH ₄		N ₂		CO ₂				
		y _i (mol/mol)	Q (mmol/g)	u(Q) (mmol/g)	y _i (mol/mol)	Q (mmol/g)	u(Q) (mmol/g)	y _i (mol/mol)	Q (mmol/g)	u(Q) (mmol/g)
333	107	0.32	0.02	0.02	0.30	0.01	0.07	0.38	2.69	0.18
	107	0.21	0.02	0.02	0.20	0.01	0.04	0.59	3.12	0.13
	107	0.11	0.01	0.01	0.10	0.00	0.03	0.79	3.57	0.10
	504	0.34	0.06	0.02	0.29	0.00	0.07	0.37	4.01	0.26
	504	0.24	0.04	0.01	0.19	0.01	0.02	0.57	4.45	0.19
	504	0.14	0.03	0.04	0.09	0.01	0.02	0.77	4.52	0.14
	902	0.37	0.11	0.00	0.28	0.00	0.04	0.35	4.33	0.31
	902	0.27	0.08	0.01	0.18	0.00	0.04	0.55	4.56	0.21
	902	0.15	0.05	0.02	0.09	0.01	0.01	0.76	4.56	0.15
303	112	0.30	0.04	0.09	0.30	0.01	0.07	0.40	3.33	0.19
	107	0.24	0.03	0.04	0.19	0.01	0.04	0.57	3.90	0.15
	107	0.13	0.03	0.03	0.10	0.01	0.04	0.77	4.44	0.11
	504	0.35	0.09	0.05	0.29	0.05	0.06	0.36	4.13	0.29
	505	0.24	0.10	0.02	0.19	0.04	0.05	0.57	4.41	0.19
	504	0.14	0.07	0.03	0.09	0.03	0.06	0.78	4.68	0.14
	902	0.37	0.13	0.04	0.27	0.06	0.07	0.35	4.30	0.33
	900	0.27	0.13	0.01	0.18	0.04	0.01	0.55	4.72	0.08
	901	0.15	0.11	0.04	0.08	0.03	0.07	0.76	5.34	0.17
273	107	0.32	0.06	0.03	0.29	0.01	0.09	0.39	4.69	0.27
	106	0.22	0.05	0.01	0.20	0.01	0.04	0.58	4.89	0.18
	107	0.11	0.03	0.04	0.09	0.00	0.01	0.80	4.97	0.14
	504	0.35	0.15	0.01	0.29	0.01	0.06	0.36	5.12	0.33
	503	0.25	0.11	0.01	0.19	0.01	0.03	0.56	5.39	0.22
	503	0.15	0.07	0.02	0.09	0.01	0.04	0.76	5.52	0.17
	902	0.37	0.16	0.01	0.28	0.02	0.07	0.35	5.25	0.37
	903	0.27	0.13	0.01	0.18	0.02	0.02	0.55	5.66	0.26
	902	0.17	0.09	0.01	0.08	0.01	0.05	0.75	5.88	0.20

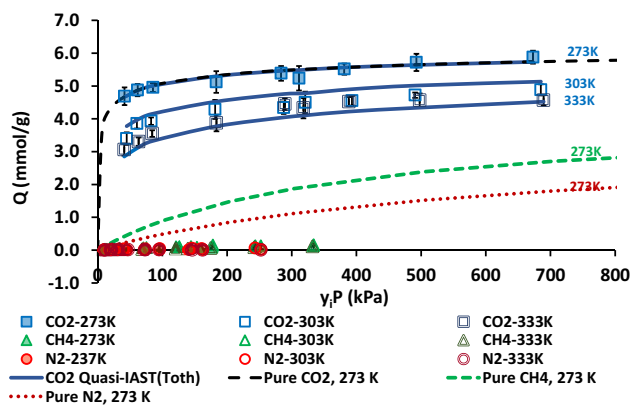


Fig. 8 Adsorption capacities for ternary gas mixture of ($\text{CH}_4 + \text{N}_2 + \text{CO}_2$) and isotherm model predictions for pure components and the same components in gas mixtures showing the impact of CO_2 on the adsorption capacity of methane and nitrogen

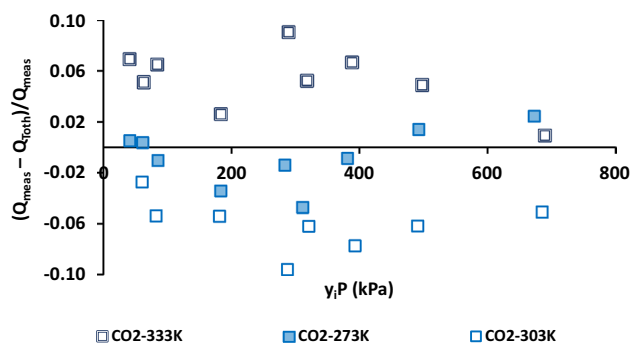


Fig. 9 Deviation plot of IAST and experimental data for $\text{CO}_2 + \text{CH}_4 + \text{N}_2$ ternary mixture as a percentage of the experimental value at three different temperatures, 333, 303 and 273 K

References

- Cavenati, S., Grande, C.A., Rodrigues, A.E.: Adsorption equilibrium of methane, carbon dioxide, and nitrogen on zeolite 13X at high pressures. *J. Chem. Eng. Data* **49**(4), 1095–1101 (2004)
- Cavenati, S., Grande, C.A., Rodrigues, A.E.: Separation of mixtures by layered pressure swing adsorption for upgrade of natural gas. *Chem. Eng. Sci.* **61**(12), 3893–3906 (2006)
- Delgado, J.A., et al.: Adsorption equilibrium of carbon dioxide, methane and nitrogen onto Na- and H-mordenite at high pressures. *Sep. Purif. Technol.* **48**(3), 223–228 (2006)
- Delgado, J.A., et al.: Carbon dioxide/methane separation by adsorption on sepiolite. *J. Nat. Gas Chem.* **16**(3), 235–243 (2007)
- Hefti, M., et al.: Adsorption equilibrium of binary mixtures of carbon dioxide and nitrogen on zeolites ZSM-5 and 13X. *Microporous Mesoporous Mater.* **215**, 215–228 (2015)
- Hofman, P.S., et al.: A dynamic column breakthrough apparatus for adsorption capacity measurements with quantitative uncertainties. *Adsorption* **18**(3–4), 251–263 (2012)
- Kidnay, A.J., Parrish, W.R., McCartney, D.G.: *Fundamentals of Natural Gas Processing*, 2nd edn. CRC Press, Boca Roca (2011)
- Kumar, K.V., et al.: A site energy distribution function from Toth isotherm for adsorption of gases on heterogeneous surfaces. *Phys. Chem. Chem. Phys.* **13**(13), 5753–5759 (2011)

- McEwen, J., Hayman, J.-D., Yazaydin, A.O.: A comparative study of CO_2 , CH_4 and N_2 adsorption in ZIF-8, Zeolite-13X and BPL activated carbon. *Chem. Phys.* **412**, 72–76 (2013)
- Mofarahi, M., Shokroo, E.J.: Comparison of two pressure swing adsorption processes for air separation Using Zeolite 5A and Zeolite 13X. *Petroleum Coal* **55**(3), 216–225 (2013)
- Mulgundmath, V.P., et al.: Adsorption and separation of CO_2/N_2 and CO_2/CH_4 by 13X zeolite. *Can. J. Chem. Eng.* **90**(3), 730–738 (2012)
- Myers, A.L., Monson, P.A.: Physical adsorption of gases: the case for absolute adsorption as the basis for thermodynamic analysis. *Adsorption* **20**(4), 591–622 (2014)
- Myers, A.L., Prausnitz, J.M.: Thermodynamics of mixed-gas adsorption. *AIChE J.* **11**(1), 121–127 (1965)
- NIST, REFPROP-Reference Fluid Thermodynamic and Transport Properties, Version 9.1. National Institute of Standards and Technology, USA (2013)
- Rao, M.B., Sircar, S.: Thermodynamic consistency for binary gas adsorption equilibria. *Langmuir* **15**(21), 7258–7267 (1999)
- Rufford, T.E., et al.: The removal of CO_2 and N_2 from natural gas: a review of conventional and emerging process technologies. *J. Petrol. Sci. Eng.* **94–95**(0), 123–154 (2012)
- Rufford, T.E., et al.: Adsorption equilibria and kinetics of methane + nitrogen mixtures on the activated carbon Norit RB3. *Ind. Eng. Chem. Res.* **52**(39), 14270–14281 (2013)
- Saleman, T.L.H., et al.: Capacity and kinetic measurements of methane and nitrogen adsorption on H^+ -mordenite at 243–303 K and pressures to 900 kPa using a dynamic column breakthrough apparatus. *Adsorption* **19**(6), 1165–1180 (2013)
- Saleman, T.L.H., et al.: A robust dynamic column breakthrough technique for high-pressure measurements of adsorption equilibria and kinetics. *Adsorption* **23**(5), 671–684 (2017)
- Sudibandriyo, M., et al.: Adsorption of methane, nitrogen, carbon dioxide, and their binary mixtures on dry activated carbon at 318.2 K and pressures up to 13.6 MPa. *Langmuir* **19**(13), 5323–5331 (2003)
- Talu, O.: Net adsorption of gas/vapor mixtures in microporous solids. *J. Phys. Chem. C* **117**(25), 13059–13071 (2013)
- Thomas, W.J., Crittenden, B.: *Adsorption Technology & Design*. Butterworth-Heinemann, Oxford (1998)
- Valenzuela, D.P., Myers, A.L.: *Adsorption Equilibrium Data Handbook*. Prentice Hall, Englewood Cliffs (1989)
- Walton, K.S., Sholl, D.S.: Predicting multicomponent adsorption: 50 years of the ideal adsorbed solution theory. *AIChE J.* **61**(9), 2757–2762 (2015)
- Wang, L., et al.: CO_2 capture from flue gas by two successive VPSA units using 13XAPG. *Adsorption* **8**, 445 (2012)
- Wang, L., et al.: Experimental and modeling investigation on post-combustion carbon dioxide capture using zeolite 13X-APG by hybrid VTSA process. *Chem. Eng. J.* **197**, 151–161 (2012)
- Watson, G., et al.: Equilibrium adsorption measurements of pure nitrogen, carbon dioxide, and methane on a carbon molecular sieve at cryogenic temperatures and high pressures. *J. Chem. Eng. Data* **54**(9), 2701–2707 (2009)
- Watson, G.C., et al.: Volumetric adsorption measurements of N_2 , CO_2 , CH_4 , and a $\text{CO}_2 + \text{CH}_4$ mixture on a natural chabazite from (5 to 3000) kPa. *J. Chem. Eng. Data* **57**(1), 93–101 (2011)
- Xiao, G., et al.: CO_2 capture at elevated temperatures by cyclic adsorption processes. *RSC Adv.* **2**(12), 5291–5297 (2012)
- Xiao, G., et al.: Adsorption equilibria and kinetics of CH_4 and N_2 on commercial zeolites and carbons. *Adsorption* **23**(1), 131–147 (2016)